JOURNAL OF MATERIALS SCIENCE 15 (1980) 1926–1938

The effect of thermal history on the crystallization kinetics of a liquid-quenched metallic glass

Part 1

P. G. BOSWELL
Dental School, University of Queensland, Turbot St., Brisbane, 4000, Australia.

The crystallization behaviour of a liquid quenched $(Ni_{0.5}Pd_{0.5})_{82}P_{18}$ amorphous alloy is not markedly affected by the imposed heating conditions. This compares with the effect of the initial quench rate such that lower quench rates stabilize the glass by raising the crystallization temperature observed on continuous heating. This stabilization is not accompanied by gross changes in the morphologies of the crystallization products.

1. Introduction

The crystallization of liquid-quenched metallic glasses has been studied extensively in recent years, and much of the work, particularly that of Chen and co-authors [1–3], has been directed to showing that the crystallization kinetics scale as the shear viscosity. Other workers have been concerned with the effects of phase separation at temperatures near T_g, the glass transition temperature, on crystallization kinetics and microstructures [4, 5]. Little attention has been given to the effects of the thermal history. In the case of liquid-quenched metallic glasses, the "history" can involve quenching at different cooling rates to a low temperature (generally room temperature). Following isothermal storage, the glasses are crystallized using isothermal or non-isothermal heat treatments.

With regard to the initial quench rate, there are several reports showing that lower quench rates tend to stabilize metallic glasses. For instance, Lewis and Davies [6] and Lasocka [7], in what appear to have been the only systematic studies of the effect of the initial quench rate, found that the temperatures T_s, corresponding to the start of crystallization under continuous-heating conditions, were more than 10 K higher for water-quenched $(Ni_{0.5}Pd_{0.5})_{82}P_{18}$ and $Te_{85}Ge_{15}$ glasses than for splat-quenched alloys. Moreover, Duhaj *et al.* [8] noted that $Pd_{80}Si_{20}$ glasses quenched from higher initial temperatures were more stable. In this case, the higher initial superheats probably gave lower quenching rates so that the change in T_s reflected, at least in part, the cooling rate effect.

There appear to be few reports of the effect of the quench rate on t_s, the isothermal heat-treatment time corresponding to the start of crystallization. Lo and Tompkins [9] in a study of the crystallization of a $Pd_{80}Si_{20}$ glass at 473 K, observed a large difference between their measured t_s time and a previously reported value. These authors attributed the discrepancy to variations in the initial melt superheats (and, by implication, the quench rates). Lo and Tompkins' result applied to the low-temperature crystallization below T_g as opposed to the high-temperature regime above T_g. There has been no report of an effect of the initial quench rate on the t_s time for crystallization at a temperature above T_g.

With regard to the effect of the imposed thermal history during reheating, it is noted that the crystallization kinetics for non-isothermal conditions have been used to predict the kinetics for isothermal conditions [2, 10, 11]. The theoretical basis of this approach has been outlined [2] but few authors have examined its accuracy. Using the limited amount of suitable data that is available we find that the measured start times t_s, for isothermal crystallization at particular temperatures above T_g agree with those calculated using continuous-heating data in the following two amorphous

0022–2461/80/081926–13$03.30/0

alloys: $Fe_{80}B_{20}$ [11] and $(Ni_{0.5}Pd_{0.5})_{80}P_{20}$ [2]. Both of these alloys probably crystallize, under isothermal and continuous heating conditions, via a single-stage process involving the nucleation and growth of micron-sized spherulites [12, 13]. Consider, on the other hand, the situation for a $Fe_{77}P_{15}C_8$ alloy, which crystallizes under isothermal conditions, and possibly under non-isothermal conditions, via two stages. The first of these stages involves the formation of submicron sized crystallites and it has been shown that the measured isothermal start times for the stage were considerably shorter than the calculated times derived using continuous-heating experiments [10]. Moreover, the kinetic data reported by Scott and Ramanchandrarao [14] for a similar alloy ($Fe_{80}P_{13}C_7$ + minor additions of Ti and Cr) can be used to show that the discrepancy also applied to the second crystallization stage. For isothermal heat treatments, the second stage involves the nucleation and growth of cellular grains and spherulites [10] similar to those observed in isothermally heat-treated $Fe_{80}B_{20}$ [12, 13] and $Pd_{78.1}Cu_{5.5}Si_{16.4}$ [15] alloys.

The results for the $Fe_{77}P_{15}C_8$ alloy, when compared with similar results for $(Ni_{0.5}Pd_{0.5})_{80}P_{20}$ and $Fe_{80}B_{20}$ alloys, suggest that the rate of formation of the fine-scale crystallization product may have been influenced by the imposed heating conditions. Any changes were then reflected in the rate of crystallization during the second stage. However, this rationale can only be justified by first showing that the mechanisms of crystallization are the same for isothermal and continuous heating. This was not done in any of the work cited above. Once it has been established that similar mechanisms are involved, it may then be possible to account for the effect of the imposed heating conditions by relating the first-stage crystallization kinetics to the structures of the relaxed glasses that are obtained on heating the as-quenched materials into the crystallization regime above T_g. It is known that the relaxation spectra of liquid-quenched metallic glasses depend upon the heat-treatment temperature, the heating rate and the initial quench rate [16].

The present communication reports upon a detailed study of the effect of the thermal history on the crystallization kinetics of a liquid-quenched metallic glass at temperatures above T_g. The communication is divided into two parts. Part I considers the effects of the initial quench rate by examining the overall crystallization kinetics and morphologies of an amorphous alloy that had been quenched at three different rates. It also investigates the effect of the imposed heating conditions by comparing the crystallization behaviour (kinetics and morphologies) in isothermally and continuously heat-treated specimens of a glass that had been prepared using a particular quenching technique. Part 2 [17] of the communication examines in detail the quench-rate dependence of the crystallization kinetics using differential thermal analysis.

In choosing a suitable alloy for the investigation it was decided to employ a $(Ni_{0.5}Pd_{0.5})_{82}P_{18}$ glass because the crystallization of this glass during continuous heating has been shown to take place via several stages [18–20]. The first involves the formation of numerous small crystals embedded in an amorphous phase. This crystallization stage has been designated MS–I′ to distinguish it from later stages that were designated MS–I″ and MS–II [20]. The MS–I″ stage has only been detected by thermal analysis in glasses prepared using relatively low quench rates: it appears to involve either the formation of a structure similar to MS–I′ or the transformation of MS–I′. The MS–II stage, on the other hand, involves the nucleation and growth of relatively few grains of a multiphase crystallization product.

It was felt that the fine-scale nature of the MS–I′ product would render its formation susceptible to the structural variations brought about by relaxation during quenching and reheating at different rates. Furthermore, the exothermic MS–I′ stage observed on continuously heating a $(Ni_{0.5}Pd_{0.5})_{82}P_{18}$ glass has been shown [19, 20] to proceed to completion prior to the sequential commencement of the MS–I″ and MS–II reactions. Quantitative differential thermal analysis can therefore be used to monitor the MS–I′ stage without the need to allow for a concurrent MS–I″ or MS–I stage. Concurrent, (or parallel), rather than sequential, crystallization reactions are thought to occur when the crystallization of the separate melts arising in a phase-separated amorphous alloy proceed in parallel rather than in series [3]. Parallel crystallization reactions have been observed in isothermally heat-treated Pd–Si based glasses [5].

2. Experimental procedure

A $(Ni_{0.5}Pd_{0.5})_{82}P_{18}$ alloy ingot was prepared using a previously reported technique which was based on conventional powder metallurgical methods.

Following homogenization and analysis, the ingot was sectioned into small pieces and the pieces were melted and resolidified using three different quenching procedures. The melt temperature prior to quenching was maintained at 1060 ± 10 K for each of the procedures. This temperature corresponded to a superheat of 150 ± 10 K above the equilibrium liquidus temperature of 910 K [19].

The three different quenching procedures were a Taylor method [21] which yielded rods having a diameter of 1.0 ± 0.1 mm; a filamentary casting method [22] which yielded 20 ± 4 μm thick ribbons; and a gun-type splat-quenching method [23] which yielded porous, 4 ± 1 μm thick splats. Details of the apparatus and techniques used in each of these casting methods have been given elsewhere [19, 20, 24] and the average cooling rates are in the order splat > ribbon > rod.

Randomly selected samples of the rod, ribbon and splat specimens were examined by X-ray diffractometry and were found to contain no detectable crystallinity. Quantitative differential thermal analysis was carried out using a micro-DTA system equipped with a pan-type, or calorimetric sample holder. The system had been calibrated previously for the effect of the linear heating rate, β, on the difference between the measured and true sample temperatures [25]; and for the temperature and sample-size dependence of h, the heat-transfer coefficient between the sample and the rest of the analysis system [26]. The magnitude of this coefficient was such that it could be adequately expressed in terms of a linear equation [27] in δT, the differential temperature signal, rather than in terms of a more accurate quadratic expression [28]. Use of the coefficient permitted x, the fraction transformed within a given exothermic peak, to be calculated from the differential temperature signal using the following expression [29]

$$x = [(c/h) \cdot \delta T + a]/A \qquad (1)$$

where c is the specific heat of the sample, A is the total area of the peak and a is the area under the peak up to a given temperature within the peak. For c/h small, Equation 1 reduces to $x = a/A$. It should be pointed out that the correction for a finite heat-transfer coefficient was small. Hence, in those cases in which the correction could not be applied, the assumption that x was proportional to a did not introduce large errors.

Temperatures during thermal analysis were measured accurate to ± 0.2 K and reported values of specific kinetic parameters correspond to the average of four separate determinations. The sample weight was usually 25 ± 1 mg although in certain cases the weight was adjusted in accordance with certain principles that are discussed below. Thermal analyses were conducted under argon in order to inhibit oxidation of the specimens. The parameters describing the crystallization kinetics of the three types of amorphous specimens were extracted from the DTA traces using a computer-driven digitizer system. Selected ribbon and splat samples were also quenched from different points along the DTA thermograms using a blast of chilled argon. The structures of these continuously-heated specimens were then investigated by transmission electron microscopy. In the case of the ribbon specimen, thin foils suitable for examination by TEM were prepared using a conventional electropolishing technique. The splat specimens, on the other hand, were examined directly.

The crystallization kinetics for isothermal conditions were measured using quantitative transmission electron metallography. The measurements were restricted to ribbon specimens which had been heat treated by immersion for various times in salt baths maintained at selected temperatures above T_g. In the case of short heat-treatment times (< 10 minutes) the ribbons were placed directly in the baths; for longer heat treatments they were sealed in evacuated pyrex capillaries.

3. Results

3.1. Continuous heating

3.1.1. Differential thermal analysis

Fig. 1 gives examples of the DTA thermograms that were obtained on heating rod, ribbon, and splat specimens at 10 K min^{-1} and a ribbon specimen at 5 K min^{-1}. In the case of the splat specimens, the inflexion corresponding to the glass transition was followed by a small exothermic peak, labelled MS–I′, and a large exothermic peak. This latter peak was found to be composed of two peaks, the smaller of which appeared as a shoulder on the leading (low temperature) edge of a large peak. This smaller sub-peak was designated MS–II while the larger sub-peak corresponded to the transformation of the fully crystallized alloy [19].

This general reaction scheme also applied to the ribbon and rod specimens. The most significant additional feature for these specimens was the appearance of a small peak, designated MS–I″, lying between the MS–I′ and MS–II peaks. The

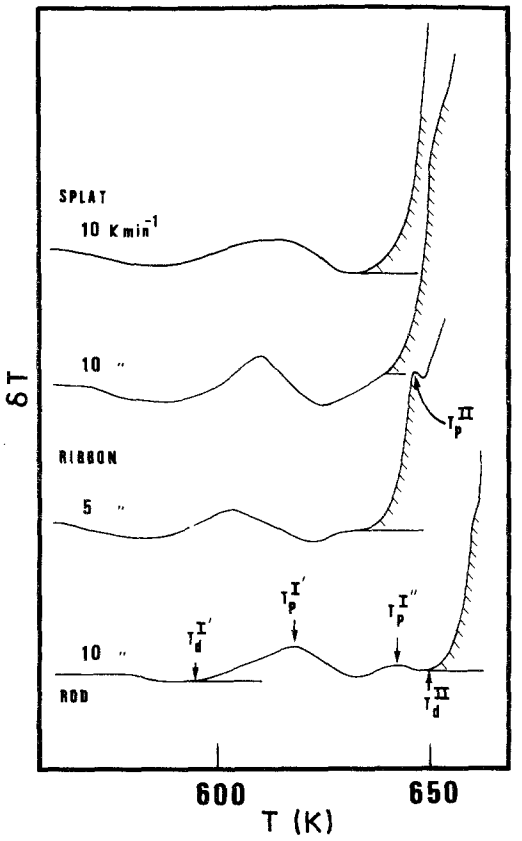

Figure 1 Representative DTA thermograms for rod, ribbon and splat-quenched $(Ni_{0.5}Pd_{0.5})_{82}P_{18}$ amorphous alloys.

MS–I″ peak was well defined in rod specimens heated at low rates ($\beta < 10\,K\,min^{-1}$) but became weaker and tended to merge with the MS–II peak in ribbon specimens and in rod specimens heated at relatively high rates ($> 10\,K\,min^{-1}$). There was no evidence for the MS–I″ exotherm in splat-quenched specimens.

3.1.2. Kissinger plots

The non-isothermal transformation kinetics were investigated using the Kissinger method [30]. This method involves plotting $\log(T_x^2/\beta)$ as a function of $1/T_x$ where T_x is the temperature corresponding to a fraction transformed, x. In the case of the MS–I′ stage, Kissinger plots were obtained for start temperature, T_s, at which $x = 0.05$, and for T_m temperatures corresponding to the maximum rate of transformation (i.e. $d^2x/dt^2 = 0$). It has been shown [19, 31] that the fractions transformed at T_m are approximately constant for different heating rates provided that the transformation rate equation under non-isothermal conditions satisfies certain conditions. In the case of the MS–I″ stage, the peak was so small that it was impractical to use it to monitor the transformation kinetics. The effect of a finite heat transfer was therefore ignored and T_m was assumed to be equal to T_p, the peak temperature.

In the case of the MS–II stage, the total area under the peak could not be evaluated owing to overlap with the transformation peak. Consequently, the fraction transformed in the course of the MS–II stage could not be calculated using the normalized area under the peak up to a given temperature (Equation 1). The temperature T_m was therefore set equal to T_p and T_s was set equal to T_d, the temperature at which the DTA curve deviated from its baseline. While both these approximations ignore the effect of the finite heat-transfer coefficient, the second approximation, like the first, requires that the fractions transformed at T_d were independent of the heating rate. Equation 1 implies that for h large and x small, the rate of change with time of the fraction transformed, dx/dt, is proportional to $\delta T/A$. Hence, if A, the total peak area, is kept constant for different heating rates by adjusting the sample weight, the temperature T_d corresponds to the temperature at which dx/dt attains a constant value that is given by the sensitivity of the analysis system. It will be shown in Part 2 of the present communication that x at t_d is approximately constant if dx/dt is constant at this temperature. Hence T_d satisfies a general requirement of the Kissinger method that the fraction transformed at the selected temperature is not strongly dependent on the heating rate.

In the present study, it was found that efforts to establish a constant x at T_d by adjusting the sample weight for different β were invalidated by the large errors associated with the identification of T_d. However, since the estimated MS–II peak areas for a sample weight of 25 mg did not vary greatly over the range of heating rates used, the assumption that x at T_d was independent of β was thought to be not unreasonable.

Identification of T_d for the MS–II stage in ribbon and rod specimens sometimes required allowance for overlap with a MS–I″ peak. An example of this overlap is shown by the DTA thermograms of Fig. 1 for a ribbon specimen heated at $5\,K\,min^{-1}$. In the case of splat-quenched specimens, it was assumed that the deviation from a horizontal baseline corresponded to the onset of the MS–II stage. This deviation may have also corresponded to the onset of a concurrent MS–I″

reaction, there being no identifiable MS–I″ peak for the splat specimens. However, on the basis of the large observed difference between the effective activation energies for the MS–I″ and MS–II stages [20], we would have anticipated the development of a MS–I″ sub-peak at low heating rates if the start temperatures for MS–I″ and MS–II coincided in splat specimens heated at high rates. No such peak developed so it is likely that either a MS–I″ stage did not occur in these specimens or the MS–I″ start temperature was not coincident with the MS–II start temperature but was displaced to higher temperatures.

Kissinger plots for the MS–I″ and MS–II stages in the three types of specimens are given in Fig. 2. These plots were obtained using T_s (or T_d) and T_m (or T_p) temperatures and they show systematic variations in a) the gradients, b) the intercepts, and c) the horizontal displacements between plots for T_s (or T_d) and T_m (or T_p) temperatures for a given stage. These variations can be analysed in terms of changes in the kinetic parameters appearing in the Avrami equation for transformation under isothermal conditions. The evaluation of these parameters using the non-isothermal DTA measurements of Fig. 2 is considered in Part II.

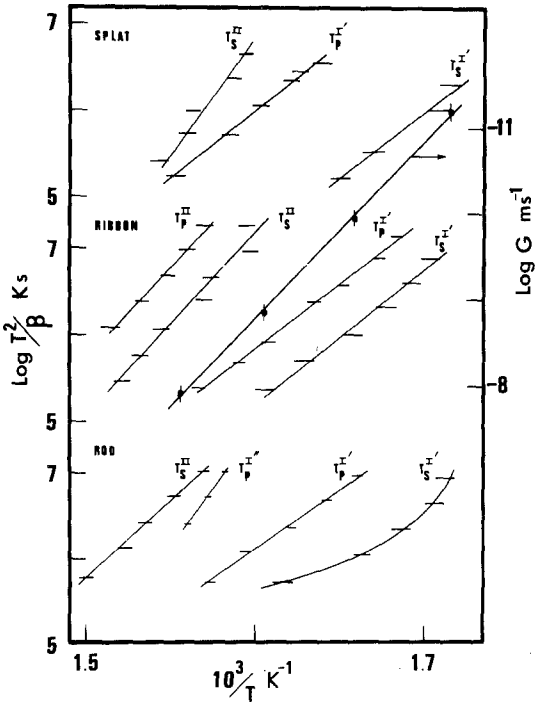

Figure 2 Kissinger plots for the MS–I′, MS–I″ and MS–II crystallization stages in rod, ribbon and splat-quenched specimens. Note that in the case of the MS–II stage, the temperatures T_s and T_m were set equal to T_d and T_p, the deviation and peak temperatures respectively.

3.1.3. Transmission electronmetallography of filamentary cast ribbons: microstructures

Fig. 3 shows TEM bright-field micrographs of representative crystallization structures observed after heating a ribbon specimen at 5 K min^{-1} to T_p (MS–II). Some areas (Fig. 3a) of the continuously heated, and electropolished, ribbons were found to contain MS–II spherulites growing into a partially crystalline matrix comprising small (<5 nm diameter) MS–I crystals embedded in an amorphous matrix. It should be noted that the prime and double-prime superscripts have been dropped form this discussion of the MS–I stage because electron microscopy showed no resolvable differences between structures obtained on heating ribbons to the end of the MS–I′ and MS–I″ peaks. This result possibly implies that the MS–I″ exotherm involved a transformation of the structure produced during the MS–I″ exotherm. Alternatively, the MS–I″ stage may have been due to the formation of additional microcrystals, similar in size to, and indistinguishable from, those microcrystals formed during the MS–I′ stage.

An enlargement of a BF image of the matrix material adjacent to the spherulite shown in Fig. 3a is given in Fig. 3b. This enlarged image shows contrast variations reminiscent of an interconnected phase-separated structure. The average wavelength of the variations are of the same order of magnitude as the measured [4] wavelengths of phase-separated structures that have been observed in Pd–Si based amorphous alloys [1]. Diffraction patterns taken from the matrix contained sharp rings superimposed on diffuse rings: these diffraction effects are described in detail in Section 3.2.1.

With regard to the MS–II structure, it should be noted that the MS–II grain imaged in Fig. 3a corresponds to a section through a spherulitic structure. Spherulites are characterized by a radiating array of radially growing crystals and spherulitic growth requires the continued nucleation of new crystals, or the subdivision of existing ones, in order to fill space. However, it was observed that thin-foil regions close to partially crystallized regions, such as the region imaged in Fig. 3a, were sometimes fully crystallized. Moreover, the MS–II structure in these areas (see Fig. 3c) was not spherulitic but appeared to comprise a dendritic arrangement of the constituent

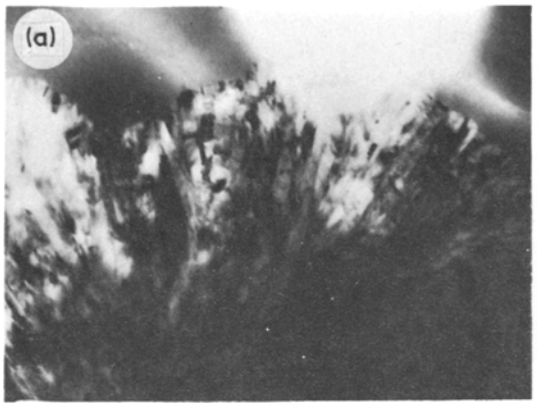

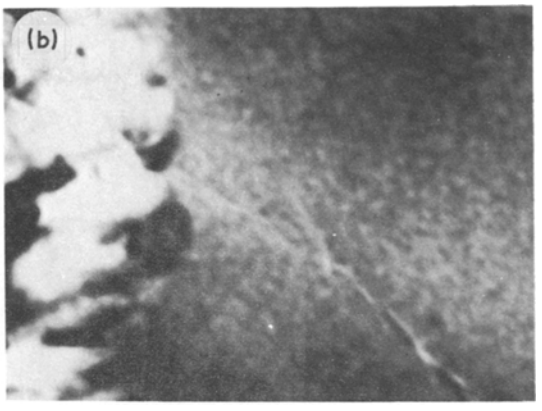

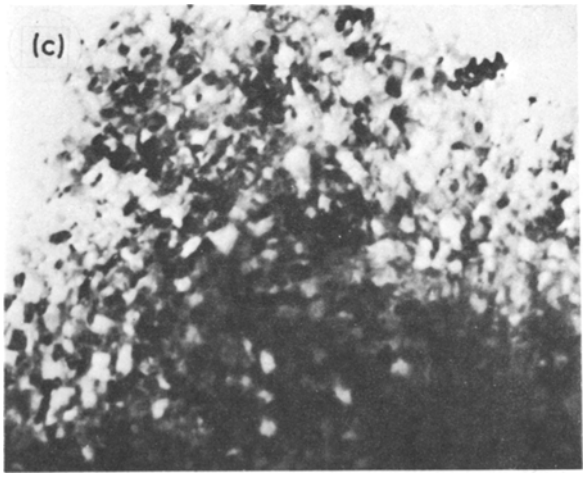

Figure 3 Ribbon specimen heated at 5 K min^{-1} to T_p (MS–II). (a) Spherulitic MS–II; (b) matrix material containing MS–I microcrystals; (c) fully crystallized, dendritic MS–II structure (the magnifications are (a) × 20K, (b) × 80K and (c) × 25K).

phases within each of the MS–II grains. The tendency for dendritic rather than spherulitic growth increased as the heating rate increased. Hence ribbons heated at 1.25 K min^{-1} contained only spherulites while ribbons heated at 20 K min^{-1} contained no spherulites. Intermediate heating rates (e.g. 5 K min^{-1}: Fig. 3) led to competition between spherulitic and dendritic crystallization. It is, of course, possible that small compositional and structural changes [13] across the filamentary cast ribbons resulted in the two different MS–II morphologies within the same electropolished thin-foil specimen. However, these features would not account for the transition from completely spherulitic to completely dendritic crystallization with an increasing heating rate. This transition must therefore be a true effect of the heating rate.

3.1.4. Filamentary cast ribbons: T–T–T diagram

The effect of β on the MS–II microstructure can be summarized by first constructing a time–temperature transformation diagram using the Kissinger plots. The construction follows from the following relationship, derived by Chen [3], between t_s and T_s:

$$t_s(T_s) = (T_s^2/\beta)/g_s$$

where $t_s(T_s)$ is the isothermal start time at T_s; T_s is the non-isothermal start temperature for a linear heating rate β; and g_s is the gradient of the $\ln(T_s^2/\beta)$ versus $1/T_s$ Kissinger plot. Both t_s and T_s refer to the same fraction transformed ($x = 0.05$ in the present study or an x value of a similar, and approximately constant, value if T_d is used instead of T_s). Fig. 5 gives the calculated T–T–T curves for the $(Ni_{0.5}Pd_{0.5})_{82}P_{18}$ ribbons together with indications of the regimes corresponding to the crystallization of dendritic and spherulitic MS–II structures.

3.1.5. Splat-quenched foils

Fig. 4 gives a TEM micrograph of a splat-quenched foil that had been heated at 5 K min^{-1} to T_p (MS–II). The MS–II structure imaged in the micrograph resembles a two-dimensional spherulite and it has essentially the same structure as the three-dimensional spherulite of Fig. 3. The matrix surrounding the MS–II spherulite displays corrugated contrast variations which were probably caused by changes in the foil thickness due to rumpling. This rumpling was presumably brought about by development of surface instabilities on heating the foil above T_g. The structure of the matrix was masked to some extent by the rumpling, and also by a

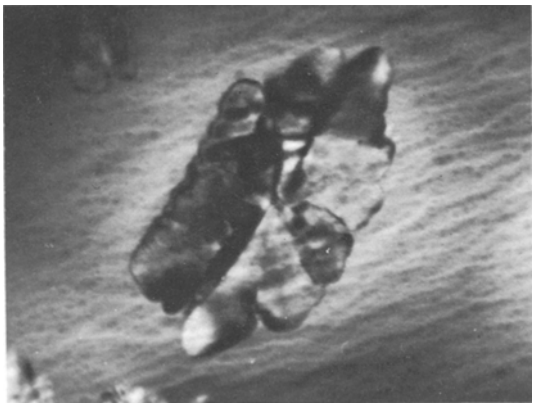

Figure 4 Splat-quenched specimen heated at 5 K min^{-1} to T_p (MS–II): two-dimensional MS–II spherulite with matrix material showing surface rumpling and contrast due to MS–I microcrystals.

small amount of surface oxidation. In spite of these artifacts it was established that the matrix imaged in Fig. 4 gave a diffraction pattern having sharp rings superimposed on diffuse rings. It was therefore concluded that the MS–I stages in the splats and ribbons involved similar crystallization mechanisms.

3.2. Isothermal heat treatment

3.2.1. MS–I crystallization

The evolution of the MS–I microstructure was monitored using ribbons that had been isothermally heat treated for progressively longer times at several temperatures above T_g. Fig. 6 shows a series of microdensitometer traces of selected area diffraction patterns that were taken following heating at T_g + 8 K. The T_g temperature (575 K) is the value obtained on extrapolating measured T_g's to a zero heating rate [25]. The traces were obtained using patterns having approximately equal intensities of the first diffraction ring so that comparisons could be made between the relative intensities of the first and second rings. The 20 minute pattern appeared to be the same as the pattern for the as-quenched glass whereas Fig. 6 shows that ageing for 2.8 h gave an increase in the relative intensity of the first ring. This intensification was accompanied by a decrease in the width of the first ring and the development of a pronounced shoulder on the second ring. The 67 h trace (Fig. 6) and its corresponding pattern (Fig. 7a) show that the second ring had developed into a sharp ring superimposed on a diffuse ring. In addition, the first ring had become narrower; its relative intensity had increased; and the maxima of the first ring and

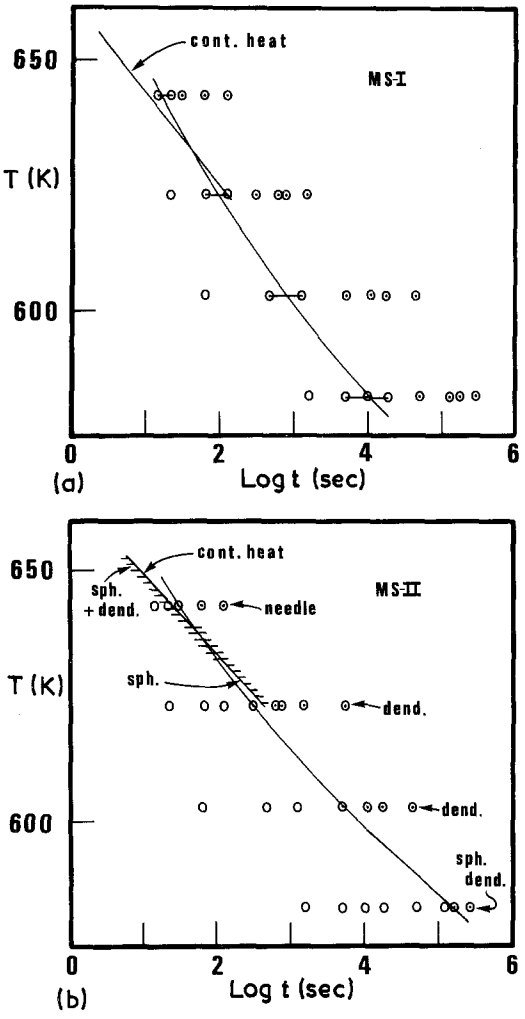

Figure 5 Time–temperature transformation diagrams for the crystallization of $(Ni_{0.5}Pd_{0.5})_{82}P_{18}$ amorphous ribbons. (a) MS–I'; (b) MS–II. The continuous heating start times were calculated using the Kissinger plots of Fig. 2.

of the sharp ring superimposed on the second ring corresponded to larger d-spacings than for the as-quenched glass. The sharp ring was produced by coherent scattering from numerous small regions embedded in the amorphous matrix. These regions were the MS–I microcrystals and they could be discerned in BF micrographs (Fig. 7b). The observed changes in the diffraction patterns for the isothermally heat-treated $(Ni_{0.5}Pd_{0.5})_{82}P_{18}$ ribbons are qualitatively similar to those described by Takayama and Maddin [32] for continuously heated, thin-foil specimens of a $(Ni_{0.6}Pd_{0.4})_{90}P_{10}$ alloy.

Chen [18], using thermal analysis, has suggested that $(Ni_{0.5}Pd_{0.5})_{82}P_{18}$ glasses phase separate near or above T_g to give two melts having different Ni

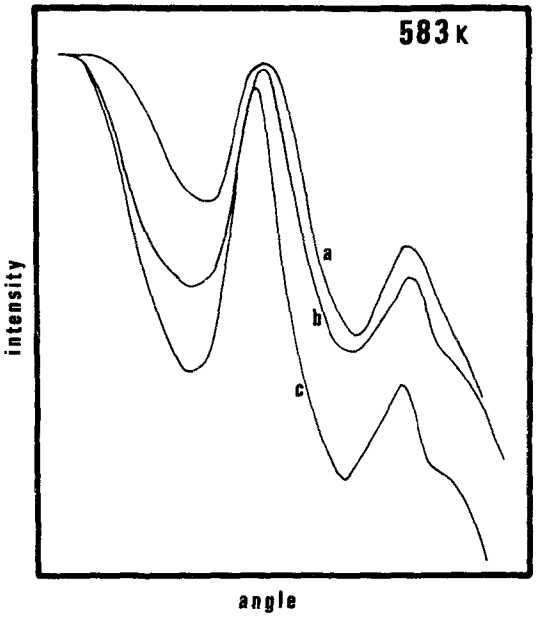

Figure 6 Microdensitometer traces of selected area diffraction patterns taken following the isothermal heat treatment of ribbon specimens at T_g + 8 K; (a) 20 min, (b) 2.8 h, (c) 67 h.

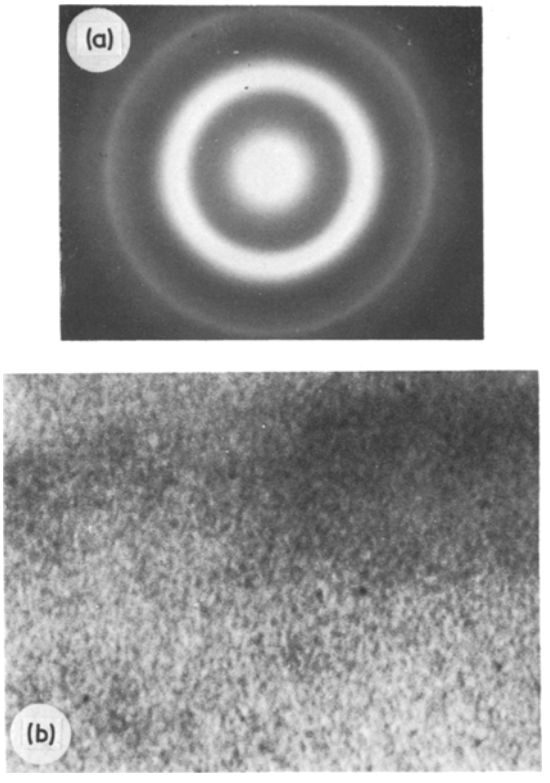

Figure 7 MS–I structure following isothermal heat treatment of a ribbon specimen at T_g + 8 K for 67 h. Diffraction pattern (a) contains sharp rings superimposed on diffuse rings (magnification × 140 K). See also Fig. 6.

and Pd concentrations and approximately equal P concentrations. He then argued that the MS–I crystallization reaction took place in one of the two melts. Moreover, previously reported [20] results showing the operation of two MS–I stages (namely MS–I′ and MS–I″) in slowly quenched $(Ni_{0.5}Pd_{0.5})_{82}P_{18}$ alloys were interpreted in terms of the crystallization of both melts. It is therefore of interest to examine whether or not the diffraction effects preceding the development of coherent scattering are in agreement with Chen's proposal.

Analysis [33] of the structures of Ni–P glasses have shown that on decreasing the metalloid content, the d-spacing corresponding to the first peak of the experimental radial distribution function extrapolated to the Goldschmidt radius for the metal component. Assuming that this is also the case for Pd–P glasses and assuming similar rates of increase in the peak positions (r_1) on adding phosphorus to amorphous Ni and amorphous Pd, it is predicted that a $(Pd)_{82}P_{18}$ glass will have an r_1 value of 0.280 nm as compared with a measured r_1 of 0.254 nm for a $(Ni)_{82}P_{18}$ glass. Liquid–phase separation with the P concentration invariant would therefore broaden the first diffraction ring. The detection of broadening of this order of magnitude using selected area diffraction would require a careful microdensitometric examination of a series of diffraction patterns taken using a range of exposures [34]. It is hoped that such a study will be made in the near future.

The observations showing that the MS–I stage involved the development of sharp diffraction rings having d-spacings that were larger than the as-quenched glass can be interpreted in terms of the formation of progressively larger amounts of crystallites having a composition that was different to that of the glass. An examination of the equilibrium phase diagrams for the binary Ni–Pd, Ni–P and Pd–P systems indicate that Ni–P alloys form a continuous series of solid solutions whereas Ni–P and Pd–P alloys display negligible terminal solid solubilities at temperatures below 600 K. The room-temperature lattice parameters of Ni and Pd are 0.352 and 0.388 nm respectively and there is only a small deviation from Vegard's Law for Ni–Pd solid solutions. It is therefore envisaged that the MS–I′ stage involved the formation and growth of a Pd–rich cubic phase in the Pd–rich phase-separated liquid, and that growth was controlled by the long-range diffusion of phosphorus. Some segregation of Ni may also have taken place during

growth of the MS–I′ microcrystals but in view of the mutual equilibrium solubility of Ni and Pd, the amount of Ni segregation was probably small. It will be demonstrated in Part 2 that a model based on long-range, solute diffusion control is in agreement with the results of an analysis of the MS–I′ crystallization kinetics.

3.2.2. MS–II crystallization

MS–II grains, or cells, observed in the isothermally heat treated ribbons displayed essentially the same types of structures as those observed in the continuously heat-treated specimens. Once again there was a systematic change in the MS–II morphology although for isothermal conditions, it varied with the crystallization temperature instead of with the heating rate.

At a low crystallization temperature (T_g + 8 K) the ribbons contained MS–II spherulites (Fig. 8a). At intermediate temperatures (Fig. 8b, T_g + 28 K) the MS–II cells were dendritic in that they comprised a few (generally only one and seldom more than three) dendrites of a phosphide phase embedded in polycrystalline material. There was also a tendency in this temperature regime for the evolution of cellular-dendritic structures from dendritic structures. For example, Fig. 8d shows that a portion of a dendritic cell had developed into a regular arrangement of parallel dendrite arms. At high crystallization temperatures (T_g + 68 K) the MS–II grains comprised needles of the phosphide phase with rows of epitaxially nucleated grains strung along two sides of each of the needles (Fig. 8e). This needle structure is also shown in Fig. 8f which is an image of a section through the mid-plane of a needle with its lobes of epitaxial grains.

Detailed studies of the crystallography and microstructures of the various types of MS–II cells indicated that the needle-like, dendritic, cellular-dendritic and spherulitic growth forms could be rationalised in terms of the growth of phosphide arms with epitaxial nucleation of the intervening grains. The various growth morphologies merely reflect the ease of formation of additional phosphide arms. At high temperatures, little or no dendrite arm branching occured and the phosphide grew as a needle. Lower temperatures led to dendrite branching and the development of equi-axed cells containing a single phosphide dendrite. Still lower temperatures gave the formation of additional arms due to such processes as twinning, the incorporation of growth defects and the nucleation of additional phosphide dendrites. Occasionally, a growing dendrite developed into regular (or cellular) dendrites. The formation of new arms and the development of regular arrays became very pronounced near T_g and the MS–II cells grew spherulitically.

3.2.3. MS–II growth rate

The isothermal growth rates of MS–II cells in the ribbon specimens were determined using the maximum section-radius method. In the case of needle-like MS–II morphologies the half-length of the phosphide needle was used instead of the radius. Fig. 9 gives plots of the cell dimensions as a function of the total heat-treatment time. It can be seen that the growth rates at the four crystallization temperatures display linear kinetics: the linear growth rates are plotted in Fig. 2 as a function of 1/T.

3.2.4. Isothermal T–T–T diagram

An isothermal start curve for the MS–I stage was estimated by identifying the time for the first appearance of the pronounced shoulder on the second diffraction ring (see Fig. 6). The experimental scatter associated with these times is relatively large so the times are given by error bars in the T–T–T diagram of Fig. 5a. A line drawn through the bars locates an approximate t_s curve. It should be pointed out that only a small proportion of the scatter associated with the t_s times is attributable to the quantification of the times at which shoulders developed. The remaining proportion of the scatter was probably due to small differences in the compositions and thermal histories of different parts of the filamentary-cast ribbons [13].

Examination of Fig. 5a indicates that the measured t_s times agree with inferred times obtained using the continuous-heating measurements. The assumption that the start of the MS–I′ exotherm corresponded to the development of a pronounced shoulder in the second diffraction ring was therefore reasonable. Moreover, a previously reported discrepancy [10] between isothermal and non-isothermal start times for MS–I stages probably reflected difficulties in identifying the structure corresponding to the start of the MS–I stage.

Fig. 5b gives the times for the first appearance of MS–II cells in the isothermally heat-treated ribbons. It can be seen that there is good agreement

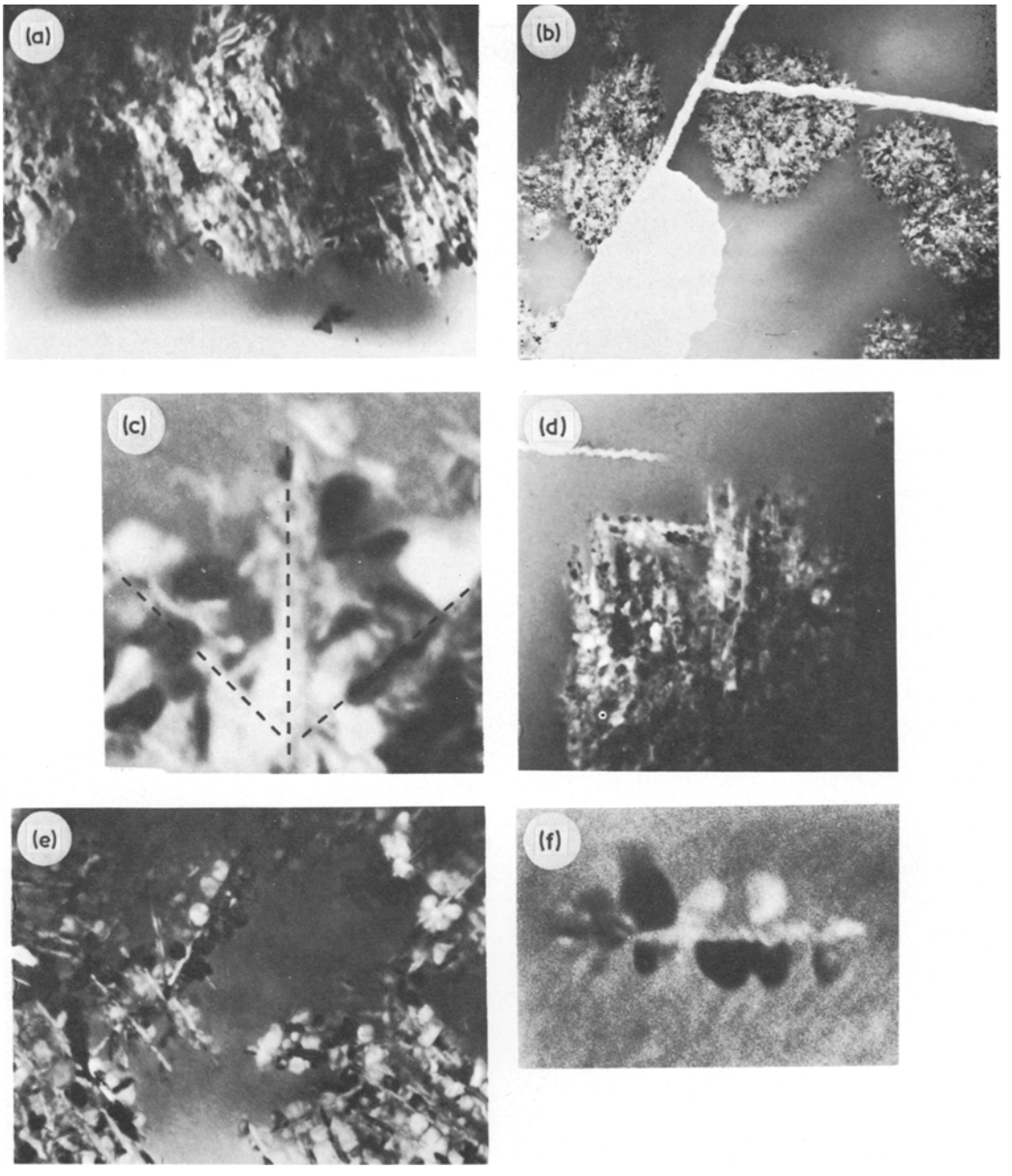

Figure 8 Isothermal MS–II structures showing the transition from rod to spherulitic to needle-like growth as the crystallization temperature increased. (a) T_g + 8 K, spherulitic (× 31 K); (b) T_g + 28 K, dendritic (× 20 K); (c) enlargement of Fig. 8b showing growth by repeated nucleation on a phosphide dendrite; (d) T_g + 28 K, partly cellular-dendritic (× 21 K); (e, f) T_g + 68 K (× 25 K, × 126 K respectively).

between these times and the times calculated using the DTA exotherms. Hence neither the MS–I′ nor the MS–II kinetics appear to show a strong dependence on the imposed heating conditions. The MS–II growth morphology, on the other hand, was found to be a function of the imposed heating conditions. This can be seen in Fig. 5b which summarizes the temperature regimes for the various MS–II morphologies that were observed in the isothermally heat-treated ribbons. By comparing these regimes with those for the continuously heat-treated ribbons, it is immediately apparent that continuous heating displaced the spherulitic–dendritic transition to a higher temperature. This

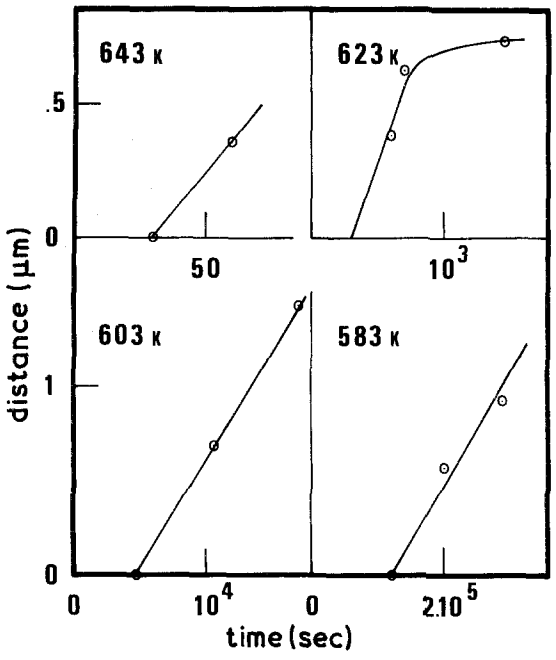

Figure 9 MS–II growth kinetics in ribbon specimens at four crystallization temperatures. Linear growth rates are plotted in Fig. 2.

change, in view of the dominating influence of the phosphide dendrite morphology on the growth morphology of an entire MS–II cell, was presumably caused by the more rapid formation of phosphide arms in the continuously heated specimens. The origin of this enhanced growth instability is not fully understood. However, an important contributing factor may be an intensification of temperature gradients at MS–II interfaces during continuous heating. These gradients would tend to destabilize cellular interfaces and thereby promote spherulitic growth.

4. Discussion

4.1. Quench rate effects

The quench rates for the three types of specimens that were examined in the present study can be estimated using reported experimental and theoretical results. In the case of the splat-quenched foils prepared by the gun technique, quenching was conducted in a vacuum using an abraded copper substrate. The heat-transfer coefficient at the splat-substrate interface was therefore $\simeq 10^6 \mathrm{Wm^{-2}K^{-1}}$ [36] and the calculated average cooling rate, assuming Newtonian cooling conditions, for the $4 \pm 1\,\mu m$ thick splats was $2 \times 10^7 \mathrm{Ks^{-1}}$ at a temperarture midway between the initial melt temperature and the glass transition temperature. An attempt was made to minimize the effects of local variations in the cooling rate thoughout the splats by selecting only those areas having thicknesses lying within the specified range. Moreover, variables such as the diaphragm rupture pressure and the orifice diameter that determined the cooling rate were kept constant.

The heat transfer coefficient for the abraded copper substrates used in casting the $20 \pm 4\,\mu m$ thick ribbons was $\simeq 10^5 \mathrm{Wm^{-2}K^{-1}}$ [37], so the average Newtonian cooling rate was calculated to be $4 \times 10^5 \mathrm{Ks^{-1}}$. It should be noted that the filamentary cast ribbons remained attached to the quenching substrates during cooling to room temperature. The ribbons therefore, did not experience a dramatic decrease in their cooling rate owing to detachment from the substrates at a relatively high temperature.

In the case of the water-quenched, glass-coated rods, the results given by Kavesh [37] indicated that axial heat flow could be ignored; that the heat-transfer coefficient at the glass-water interface was $\simeq 6 \times 10^4 \mathrm{Wm^{-2}K^{-1}}$; and that the cooling behaviour of the glass coated rods was approximately Newtonian. Assuming perfect thermal contact at the glass-metal interface, we can use an expression given by Pardoe *et al.* [38] to calculate an average cooling rate of $5 \times 10^3 \mathrm{Ks^{-1}}$. The cooling rates for the three types of amorphous $(Ni_{0.5}Pd_{0.5})_{82}P_{18}$ specimens were therefore in the expected [6] order (i.e. splat > ribbon > rod) and there was likely to have been an appreciable difference between the cooling rates for each of the three specimen configurations.

In agreement with results reported by other workers [6, 7], it was found that lower quench rates stabilized the $(Ni_{0.5}Pd_{0.5})_{82}P_{18}$ alloy by raising the temperature corresponding to the start of crystallization upon continuous heating to temperatures above T_g. The stabilization was accompanied by changes in the gradients, intercepts and separations of the Kissinger plots for the MS–I and MS–II crystallization stages. The significance of these changes is analysed in detail in Part 2. This analysis will be predicated on the assumption that the crystallization mechanisms were independent of the initial quench rate. The TEM results for ribbons and splats heated to different points along their respective thermograms confirmed, in general, the validity of this assumption. Any observed differences between the crys-

tallization structures for these two types of specimens largely reflected the proximities of the closely-spaced free surfaces in the splat-quenched foils.

It should be pointed out that detailed TEM studies of the MS–I crystallization structures observed following continuous heating could only be based on the examination of diffraction effects. This is because of artifacts such as accelerated crystallization [35] and micropitting produced during electropolishing, and surface rumpling and oxidation produced during the heating of splat-quenched foils, make electron metallographic techniques unsuitable. While the diffraction effects revealed an essential similarity between the structures developed during the initial crystallization stage, they did not appear to be able to shed any light on the origin of the MS–I'' sub-peak observed on heating ribbon and rod specimens at low heating rates.

4.2. Effect of the imposed heating conditions

It was established that the MS–I' and MS–II stages in the $(Ni_{0.5}Pd_{0.5})_{82}P_{18}$ alloy proceeded sequentially for both isothermal and continuous-heating conditions and that the overall crystallization kinetics (measured using the start times) were not strongly dependent on the imposed heating conditions. Chen and Coleman [16] have shown that metallic glasses probably display localized relaxation at low temperatures and co-operative, long-range relaxation at high temperatures. The crystallization kinetics for isothermal and continuously-heated specimens suggested that this temperature dependence of the relaxation behaviour was not reflected in any gross changes in the crystallization behaviour. Crystallization during reheating at temperatures above T_g was therefore only weakly dependent on the nature of the relaxation processes preceding crystallization; any model for the effect of the initial quench rate should be consistent with this behaviour.

With regard to liquid-phase separation, there appears to be no fundamental reason why phase separation should necessarily require parallel rather than sequential crystallization of the two melts. This supposition is supported by Chou and Turnbull's [4] results showing that a $Pd_{74}Au_8Si_{18}$ glass displayed sequential crystallization kinetics on continuous heating (isothermal crystallization kinetics were not reported for this alloy). The glass was thought to phase separate on the basis of small angle X-ray scattering measurements. Furthermore, it can be inferred from the results reported by Marcus [5] that a $Pd_{80.5}Si_{14.5}Sb_5$ glass, which phase separated and displayed parallel crystallization during isothermal heating, probably displayed sequential crystallization during continuous heating. Hence, the observation of sequential crystallization in the $(Ni_{0.5}Pd_{0.5})_{82}P_{18}$ alloy, for both isothermal and continuous-heating conditions, is not likely to be in conflict with the proposal that the alloy phase separated above T_g.

5. Conclusions

The effect of the initial quench rate on the crystallization behaviour of a liquid-quenched $(Ni_{0.5}Pd_{0.5})_{82}P_{18}$ amorphous alloy at temperatures above T_g has been examined using rod, ribbon and splat specimens that were quenched at $\sim 5 \times 10^3$, 4×10^5 and 2×10^7 Ks^{-1}.

Transmission electronmetallography indicated that the only significant difference in the crystallization morphology between ribbon and splat specimens was a modification to the structure of the second stage (MS–II) crystallization product. This modification can be attributed to the presence of closely spaced, free surfaces in splat-quenched specimens.

The overall crystallization kinetics for the three types of specimens were monitored using a Kissinger analysis of DTA thermograms. It was found that a decrease in the quench rate stabilized the glass by raising the crystallization temperature observed on continuous heating. This stabilization was accompanied by systematic variations in the gradients and intercepts of the Kissinger plots for the first (MS–I') and second (MS–II) crystallization stages. The significance of the variations will be considered in detail in Part 2.

The effect of the imposed heating conditions was examined by comparing the crystallization behaviours of continuously-heated and isothermally-heated ribbon specimens of the $(Ni_{0.5}Pd_{0.5})_{82}P_{18}$ alloy. No significant difference was found between the isothermal and continuous-heating start times for both the MS–I' and MS–II stages. However, continuous heating increased the temperature corresponding to the transition from spherulitic to dendritic MS–II growth morphologies.

Acknowledgement

This research was undertaken while the author was attached to the Department of Mining and Metallurgical Engineering, University of Queensland.

The author is indebted to the Australian Research Grants Committee for financial support; and to Professor G. A. Chadwick for advice and encouragement.

References

1. H. S. CHEN and D. TURNBULL, *Acta Met.* **17** (1969) 1021.
2. H. S. CHEN, *J. Non-Crystalline Solids* **27** (1978) 257.
3. Idem., **29** (1978) 223.
4. C-P. P. CHOU and TURNBULL, *ibid* **17** (1975) 169.
5. M. A. MARCUS, *ibid* **30** (1979) 317.
6. B. G. LEWIS and H. A. DAVIES, Proceedings of the International Symposium on the Structure of Non-Crystalline Materials, Univ. of Cambridge, 1976 (Taylor and Francis, London 1977).
7. M. LASOCKA, *J. Mater. Sci.* **11** (1976) 1770.
8. P. DUHAJ, V. SLADĚTE and P. MRAFKO, *J. Non-Crystalline Solids* **13** (1974) 341.
9. C. C. LO and H. G. TOMPKINS, *J. Appl. Phys.* **47** (1976) 3496.
10. P. H. SHINGU, K. SHIMOMURA, R. OZAKI, K. OSAMURA and Y. MURAKAMI, Proceedings of the 3rd International Conference on Rapidly Quenched Metal, Univ. of Sussex, 1978.
11. F. E. LUBORSKY and H. H. LIEBERMANN, *Appl. Phys. Lett.* **33** (1978) 233.
12. J. L. WALTER, S. F. BARTRAM and R. R. RUSSELL, *Met. Trans.* **9A** (1978) 803.
13. U. KOSTER and U. HEROLD, *Scripta Met.* **12** (1978) 75.
14. M. G. SCOTT and P. RAMACHANDRARAO, *Mater. Sci. Eng.* **29** (1977) 137.
15. P. G. BOSWELL and G. A. CHADWICK, *Scripta Met.* **10** (1976) 509.
16. H. S. CHEN and E. COLEMAN, *Appl. Phys. Lett.* **28** (1976) 245.
17. P. G. BOSWELL, *J. Mater. Sci.* **15** (1980) 1939.
18. H. S. CHEN, *Mater. Sci. Eng.* **23** (1976) 151.
19. P. G. BOSWELL, *Scripta Met.* **11** (1977) 701.
20. Idem, **12** (1978) 673.
21. G. F. TAYLOR, *Phys. Rev.* **23** (1927) 655.
22. H. H. LIEBERMANN and C. D. GRAHAM, *IEEE Trans.: Magnetics* **MA-12** (1976) 921.
23. P. DUWEZ and R. H. WILLENS, *Trans. Met. Soc. AIME* **60** (1967) 605.
24. P. G. BOSWELL, *Mater. Sci. Eng.* **34** (1978) 1.
25. *Idem, Scripta Met.* **11**(1977) 603.
26. P. G. BOSWELL and G. A. CHADWICK, *Acta Met.* **28** (1980) 209.
27. P. BAUMGARTNER and P. DUHAUT, *Bull. Soc. Chim. France* (1960) 1187.
28. J. TATENO, Trans. Faraday Soc. **62** (1966) 1885.
29. H. J. BORCHARD and F. DANIELS, *J. Amer. Chem. Soc.* **79** (1957) 41.
30. H. E. KISSINGER, *J. Res. Nat. Bur. Std.* **57** (1956) 217.
31. D. W. HENDERSON, *J. Non-Crystalline Solids* **30** (1979) 301.
32. S. TAKAYAMA and R. MADDIN, *ibid.* **20** (1976) 123.
33. G. S. CARGILL III, *Solid State Phys.* **30** (1975) 227.
34. R. RAY and D. SZYMANSKI, *Met. Trans.* **4** (1973) 1785.
35. J.-M. VITEK, J. B. VANDER SANDE and N. J. GRANT, *Acta Met.* **23** (1975) 165.
36. H. A. DAVIES and J. B. HULL, *Mater. Sci. Eng.* **23** (1976) 193.
37. S. KAVESH, Amer. Inst. Chem. Eng. Symposium Series Number 180, Vol. 74, p. 1.
38. G. W. F. PARDOE, E. BUTLER and O. GELDER, *J. Mater. Sci.* **13** (1978) 786.

Received 3 August and accepted 5 December 1979.